EFFECTS OF MASS UNBALANCE AND HIGH LEVELS OF EXTERNAL DAMPING ON THE POST-CRITICAL FLUTTER OF A FLAT PLATE

Luca Pigolotti[+1], Claudio Mannini[+2] and Gianni Bartoli[+3]
[+1,2,3] CRIACIV/Department of Civil and Environmental Engineering, University of Florence, Italy

The post-critical flutter regime is still an open issue, despite the interest for its applications in the field of energy harvesting, where the knowledge of the self-sustained motion at large amplitudes is of crucial importance. In the paper, the experimental approach has been followed to investigate this issue. The role of some governing parameters, mainly the mass centre position and the damping level in the translational degree of freedom, were investigated through wind tunnel tests, evaluating their effects on the critical condition and subsequent oscillatory regime. Linear analyses supported the identification of the instability threshold. Downstream mass eccentricity of about 0.05 times the section chord significantly anticipated the critical onset velocity and modified the motion characteristics, in terms of ratio between translational and rotation amplitudes and their phase difference. External damping was introduced, up to a ratio-to-critical value of 18%, and the consequent reduction of the motion amplitudes was clearly shown. In particular, even if the amplitude-velocity diagrams always maintained the same qualitative features, a non-linear dependence on the damping level of its slopes was apparent. In addition, a theoretically stable configuration with large damping was found to perform self-sustained motion if triggered by large initial conditions.

Keyword: Flutter, Wind Tunnel Tests, Post-critical Behaviour, Sub-critical Bifurcation.

1. INTRODUCTION

In the common practice of wind and aeronautical engineering, dynamic fluid-structure interaction is a dangerous phenomenon and the design of structures prone to flow-induced vibrations usually aims at limiting any flow-induced vibration. Nevertheless, the aeroelastic phenomena are characterized by important nonlinear effects that produce Limit Cycles of Oscillation (LCO). In some cases, LCO is restricted to a limited range of flow velocities, as in the case of vortex-induced vibrations, or flow-velocity-unrestricted oscillations can be observed after a critical threshold, as in the case of galloping and flutter. From a different perspective, recent studies on alternative energy sources showed the possibility of exploiting fluid-elastic instabilities and the consequent large steady-state oscillations to capture energy from the flow and generate electricity through suitable energy conversion apparatus[1)]. Some authors have preliminary explored aero-/hydro-elastic generators based on: vortex-induced vibrations[2)]; transverse[3)] and torsional[4),5)] galloping; wake-galloping[6)]; flapping[7),8),9)] and fluttering[10)] wings.

From the literature analysis one can conclude that flutter-based solutions are the most promising ones[8),10)] and the actual capability of performing self-sustained large-amplitude motion in the post-critical regime is a fundamental requirement for any flutter-based generator. Nevertheless, only very few scientific works have been developed so far on the flutter post-critical regime, due to the limited interest for conventional civil/aeronautical structures. Reliable predictive models for the post-critical behaviour are still missing and CFD investigations are hardly applicable due to the very large-amplitude oscillations. Following an experimental approach, aeroelastic setups can be developed to observe the post-critical response[11)], but they require specific and complex design solutions.

In the classical flutter[12)] involving two Degrees of Freedom (DoFs), the system is excited by aerodynamic lift and moment forces depending on its motion. The energy transfer between airstream and structure relies on the elastic and/or aerodynamic coupling between two modes, generally with components on

[+1]luca.pigolotti@dicea.unifi.it, [+2]claudio.mannini@dicea.unifi.it, [+3]gianni.bartoli@unifi.it

both DoFs, as well as on the phase lag between the displacement and its aerodynamic reaction. This interaction generates phase adjustment and loss of damping in one of the modes, which leads to the instability and drives the growth of the motion. Then, when the cross-flow displacements and rotations are no longer small, nonlinearities occur in the self-excited loads. Particularly important are those due to the massive flow separation encountered for large angles of attack, beyond the dynamic stall angle of the section. The subsequent amplitude-velocity path manifests large amplitudes in both degrees of freedom that generally increase with the flow velocity, after a steep initial jump.

Unlike the availability of semi-empirical predictive models about the dynamic-stall flutter mechanism[13),14),15)], due to the importance for wings operating at high angles of attack[16),17),18),19),20)], the research on post-critical oscillations due to classical flutter is not so extensive. In addition, the physical sources of nonlinearity still represent an open issue, since the literature studies often focused on classical flutter LCOs under specific nonlinear mechanical boundary conditions[21),22),23)]. Hence, further research is required on reliable mathematical models and experimental setups allowing for large oscillations to deal with the classical-flutter post-critical behaviour.

This work concentrates on wind tunnel tests on a sectional model with elongated rectangular cross section (width-to-depth ratio of 25:1, with the smaller dimension of 4 mm facing the flow). The developed setup allowed motion in two DoFs), namely vertical (heaving, η, maximum ±100 mm) and rotational (pitching, α, maximum ±150°) oscillations, with linear mechanical features in the tested range. Magnetic dampers were used to introduce linear viscous damping into the heaving degree of freedom, up to a ratio-to-critical value of about 20%. Linear aeroelastic models were preliminary used to parametrically explore the flutter boundaries.

The main objective of the paper is to improve the understanding of the influence of some of the governing parameters on the system response[24)], such as the position of the mass centre, the ratio of pitching to heaving frequency and the still-air heaving damping. The latter, in the context of flutter-based energy generators, can be assumed to simulate the energy extraction process[25)], as it pumps out energy from the fluid-structure system.

2. METHODOLOGY

(1) Analytical linear model

The stability of the system is investigated by means of linearized models, arranged for the 2-DoF problem, within the assumption of small perturbations around the equilibrium position. The self-excited loads are given by Theodorsen's model[12)], which derives from potential flow theory applied to a theoretical flat plate in conjunction with the Kutta condition. The investigated width-to-depth ratio of the cross section is 25:1 and it is large enough for the oscillation body to be idealized as a flat plate[26)].

The 2-DoF flutter problem (Figure 1) and the governing equations are reported in a non-dimensional form in Eqs. 1-2, assuming the heaving and pitching DoFs in the form $\eta(t) = \eta^* e^{i(2\pi n t)}$ and $\alpha(t) = \alpha^* e^{i(2\pi n t - \phi^*)}$, where n and ϕ^* are respectively the frequency of oscillation and phase difference at flutter onset:

$$\begin{cases} \mu\left\{\left[\left(1+ig_{\eta 0}\right)\dfrac{X}{\gamma_n^2}-1\right]\dfrac{\eta(t)}{B}-x_m\alpha(t)\right\} = \bar{L}_{\eta,j}(\eta,\alpha,K,x_e,t) \\ \mu r_\alpha^2\left\{[(1+ig_{\alpha 0})X-1]\alpha(t)-\dfrac{x_m}{r_\alpha^2}\dfrac{\eta(t)}{B}\right\} = \bar{M}_{\alpha,j}(\eta,\alpha,K,x_e,t) \end{cases} \tag{1}$$

$$\begin{aligned} \bar{L}_{\eta,T}(t) &= -\left[-\frac{\pi}{2}+iC_L'\frac{C(k)}{K}\right]\frac{\eta(t)}{B}-\left\{\left[\frac{\pi x_e}{2}+C_L'\frac{C(k)}{K^2}\right]+i\left[\frac{\pi}{2K}+C_L'\frac{C(k)}{K}\left(\frac{1}{4}-x_e\right)\right]\right\}\alpha(t)\,; \\ \bar{M}_{\alpha,T}(t) &= \left[-\frac{\pi x_e}{2}+iC_M'\frac{C(k)}{K}\right]\frac{\eta(t)}{B}+\left\{\left[\pi\left(\frac{1}{64}+\frac{x_e^2}{2}\right)+C_M'\frac{C(k)}{K^2}\right]+i\left[-\frac{\pi}{2K}\left(\frac{1}{4}-x_e\right)+C_M'\frac{C(k)}{K}\left(\frac{1}{4}-x_e\right)\right]\right\}\alpha(t). \end{aligned} \tag{2}$$

The heaving amplitude is normalized with the plate chord (width) $B = 2b$. $g_{\eta 0}$ and $g_{\alpha 0}$ are the coefficients

of rate-independent damping[12] for the heaving and pitching DoFs, as obtained through free-vibration decays of the mechanically uncoupled system in still air, and they are used here instead of the ratio-to-critical damping $\xi_{\eta 0} = \xi_{\eta 0,S} + \xi_{\eta 0,E}$ and $\xi_{\alpha 0} = \xi_{\alpha 0,S}$. Concerning the notation of $\xi_{\eta 0}$ and $\xi_{\alpha 0}$, the subscript 'S' stands for the structural damping, while 'E' for the external damping that can be varied with the electromagnetic dampers. The parameters C_L' and C_M' in Eq. 2 are the slopes of the lift and moment aerodynamic coefficients, which for a flat plate are equal respectively to 2π and $2\pi(1/4 + x_e)$, while $C(k)$ is Theodorsen's circulatory function[12] depending on $k = \omega b/U = K/2$. The other dimensionless parameters playing a role in the flutter problem are: x_e and x_m, non-dimensional position respectively of the centre of elasticity and of the centre of mass; μ, proportional to the ratio of the mass of the model to the mass of the moved air; r_α, non-dimensional radius of polar inertia; γ_n, frequency ratio in still air of the uncoupled modes; X, unknown non-dimensional flutter frequency; $U_{R\alpha}$, reduced flow velocity or $K_{R\alpha}$ reduced frequency:

$$x_e = \frac{e}{B};\quad x_m = \frac{S_\alpha}{I_\eta B} = \frac{a}{B};\quad \mu = \frac{2I_\eta}{\rho B^2 S};\quad r_\alpha = \sqrt{\frac{I_\alpha}{I_\eta B^2}};\quad \gamma_n = \frac{n_{\alpha 0}}{n_{\eta 0}};\quad X = \left(\frac{n_{\alpha 0}}{n}\right)^2;\quad U_{R\alpha} = \frac{U}{n_{\alpha 0} B} = \frac{2\pi}{K_{R\alpha}} \qquad (3)$$

In Eq. 3: ρ is the flow density; I_η and I_α are the inertiae in the heaving and pitching DoFs, respectively; S_α is the static mass unbalance; S denotes the span of the model.

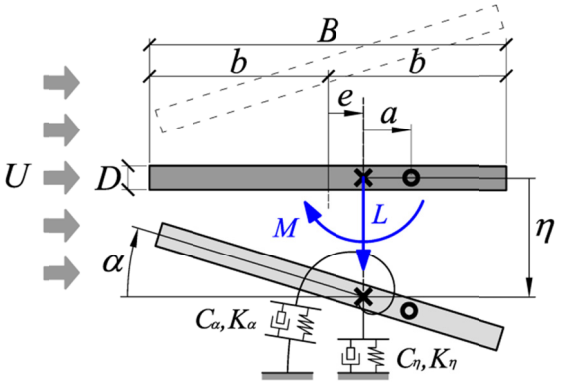

Figure 1: Sketch of the flutter problem of a two-degree-of-freedom, two-dimensional flat plate.

(2) Experimental campaign

The experimental campaign was conducted in the open-circuit, boundary layer wind tunnel of CRIACIV, in Prato, Italy. The facility is about 22 m long and the geometry of the test section is 2.41×1.60 m^2 (width×height). The 156 kW fan, placed downstream the test section, allows continuously varying the flow speed up to 30 m/s through an inverter and/or controlling the pitch angle of the rotor blades.

The aeroelastic setup (Figure 2) was specifically designed to allow large amplitudes of oscillation with linear mechanical behavior. The stiffness of the heaving DoF was controlled through the free length (1004 mm) of two pairs of aluminium beams (or blade-springs, 50 mm wide and 3 mm thick). Each pair was arranged to provide a frame with shear-type deformation thanks to a Vierendeel girder connecting the free ends of the beams, while the other ends are clamped by fixed supports. Two linear springs (the top one having a stiffness of 195 N/m and the bottom one of 95 N/m), placed outside the test section, were linked to the free ends of each frame through steel cables, in order to compensate the static deflection and contribute to the heaving stiffness. Each frame was equipped with a clock spring (with a rotational stiffness of 2.057 Nm/rad). Moreover, the model axis was connected to the elastic supporting frames by means of radial ball bearings, in order to decouple the two degrees of freedom. In addition, the connection of the flat plate to the end tube allowed to control the position of the elastic centre, while two rocker arms fixed to the model axis were devised to vary the mass centre by adding calibrated masses. Damping devices, based on the eddy-current dissipation generated on an aluminium plate (5 mm thick) moving between a pair of circular permanent magnets (neodymium N45, 35×20 mm) at close distance, were installed to introduce linear viscous damping in the heaving DoF.

The heaving motion was recorded through two analogic laser displacement transducers (measuring range of 200 mm), pointing the ends of the shear-type frames, so enabling also the monitoring of the possible rolling motion. A third laser transducer was pointing directly the model to check for a possible mean pitching rotation with increasing flow speed. Two miniaturized accelerometers were installed at the ends of one of the rocker arms to record the pitching motion up to large amplitudes. The sampling frequency during the tests was 2000 Hz.

Figure 2: Frontal view of the aeroelastic setup (top); close-ups of the damping devices (bottom-left) and of the Vierendeel girder with clock spring and hooking system for the elastic/mass centre control (bottom-right).

The suspension system was sheltered from the flow by means of two screens having a nose following the geometry of a NACA0020 profile, limiting both the disturbances produced by the setup to the incident flow and the unwanted aeroelastic effects of the oscillating supporting elements (mainly the blade-springs). Circular aluminium end-plates, 400 mm large and 1.5 mm thick, were also provided to the model ends to ensure time-averaged two-dimensional flow conditions.

The steel model had a rectangular cross section with sharp edges and it was 100 mm wide (B) and 4 mm deep (D), the smaller dimension being the one facing the wind. The free span of the model (S) was 541 mm, calculated as the distance between end-plates. The model was arranged with a nose-up angle of about 0.43° to compensate the vertical incidence of the flow in the test section. Much attention was paid to arrange the whole setup as symmetric as possible with respect to the along-wind centreline of the model in order to limit the unwanted rolling motion. The blockage ratio, calculated in a vertical plane crossing the model in the rest position, was about 0.25%. This value increased up to 6.25% when the model experienced pitching amplitudes around 90°.

The tests were conducted in smooth flow conditions with a free-stream turbulence intensity of about 0.7%. The mean flow speed was measured by means of a Prandtl tube installed upstream the model and corrected through known flow maps to infer the velocity at the model centreline. The Reynolds number (defined as $Re = UB/\nu$, with $\nu = 15$ mm^2/s) during the tests was in the range 33,000 to 107,000.

The stiffness linearity of the aeroelastic setup, both in the pitching and heaving degrees of freedom, was verified through static tests (Figure 3), measuring static displacements for different known loads. The effective inertia of the oscillating system in the heaving and pitching motions, I_η and I_α, were calculated from the previously estimated stiffness and the corresponding frequency of oscillation in still air. Dynamic tests, in which the frequencies were measured for different additional inertias, confirmed the results. Moreover, for each configuration, several free decay tests (Figure 4) were performed in still air for different initial conditions, in order to evaluate the natural frequencies of oscillation ($n_{\eta 0}$, $n_{\alpha 0}$) and the ratio-to-critical damping coefficients ($\xi_{\eta 0}$, $\xi_{\alpha 0}$). Higher levels of $\xi_{\eta 0}$ were reached through the electromagnetic system, up to a value of about 18%. The static unbalance, S_α, was estimated by measuring the frequencies of oscillation of the system during coupled pitching-heaving motion[27]. Table 1 summarises the characteristics of the tested configurations.

Table 1. Parameters of the configurations tested during the experimental campaign.

Configuration	ρ [kg/m^3]	I_η [kg]	I_α [kg·m^2]	S_α [kg·m]	$n_{\eta 0}$ [Hz]	$n_{\alpha 0}$ [Hz]	$\xi_{\eta 0}$ [%]	$\xi_{\alpha 0}$ [%]	$\boldsymbol{x_e}$ [-]	$\boldsymbol{x_m}$ [-]	$\boldsymbol{\mu}$ [-]	$\boldsymbol{r_\alpha}$ [-]	$\boldsymbol{\gamma_n}$ [-]
#1	1.15	8.058	0.03147	0.073	1.886	1.820	0.05	1.67	0.00	0.091	2708.9	0.625	0.965
#2	1.17	7.867	0.03165	0.045	1.731	1.814	0.04	1.24	〃	0.057	2604.7	0.634	1.048
#2a	1.16	〃	〃	〃	〃	〃	9.52	〃	〃	〃	2615.4	〃	〃
#2b	1.17	〃	〃	〃	〃	〃	18.13	〃	〃	〃	2605.3	〃	〃
#3	1.16	7.872	0.02902	0.000	1.731	1.895	0.05	1.23	〃	0.000	2617.1	0.607	1.095
#3a	1.15	〃	〃	〃	〃	〃	9.52	〃	〃	〃	2660.6	〃	〃
#4	1.16	〃	0.03165	0.045	〃	1.814	0.05	1.24	〃	0.057	2627.6	0.634	1.048

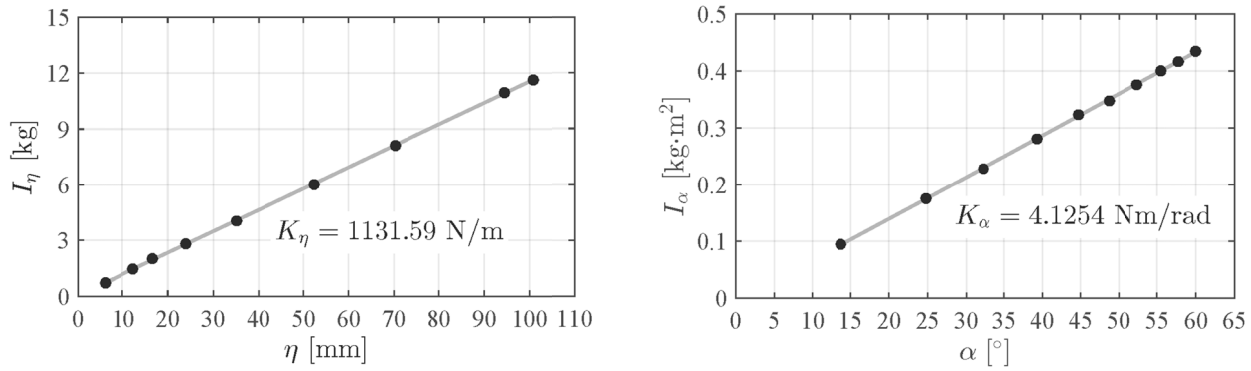

Figure 3: Static measurements to verify the linearity of heaving (left) and pitching (right) stiffnesses.

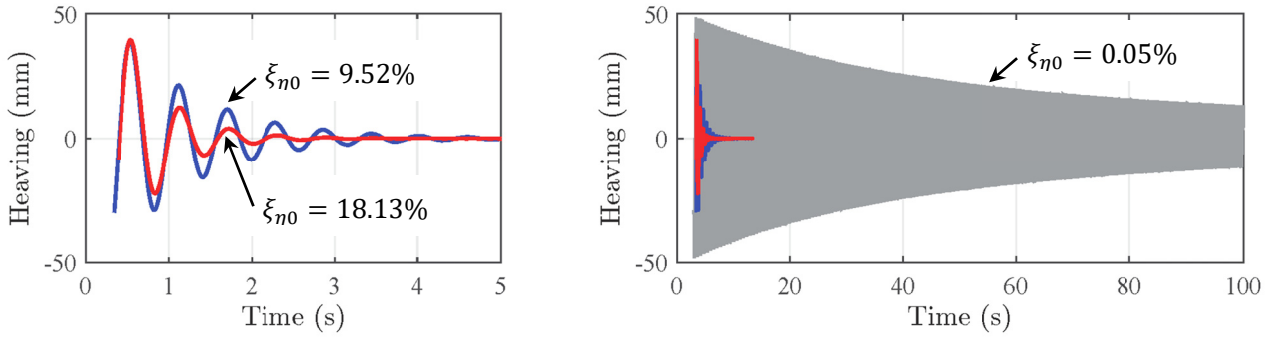

Figure 4: Example of free-decay tests for high levels of heaving damping (left) and comparison with the free-decay oscillation in the case of structural damping only (right).

3. RESULTS

The experiments were conducted in a systematic way. For each configuration, the estimation of the critical condition was theoretically conducted on the basis of the governing parameters, as obtained from the system identification, and then compared with those experimentally observed. Several initial conditions with different amplitudes were released for some flow velocities close to the theoretical flutter boundary, in order to get information on the unstable branch position, separating up to the critical threshold the stable rest position and the stable subcritical branch of the amplitude-velocity path. Indeed, as a general result, all configurations featured an instability mechanism with sub-critical bifurcation. After the flutter onset, the build-up of the oscillation was registered (Figure 5), identifying a transition regime in which the system markedly adjusts its response with respect to the nonlinear aeroelastic loads due to the large-amplitude motion. The following amplitude-velocity path was recorded for a time long enough (about 200 s) both to allow the stabilisation of the LCO amplitudes and to achieve a frequency resolution in the spectra to correctly detect the frequency peaks even at close distance. Amplitude-velocity points with increasing and decreasing flow speed were observed, up to the end of the sub-critical branch when the oscillation died out.

As predicted by the linear theory, the instability threshold is significantly anticipated in the case of small positive mass eccentricity (Figure 6). Moreover, comparing configurations #3 and #2, the sole modification of x_m importantly changes the characteristics of the motion. The phase ϕ^* varies from 12° to 152°, moving the region in which the motion centre of rotation lies from upstream to downstream the midchord. The motion components are strongly modified as well, producing larger pitching-heaving amplitude ratios $B\,\alpha^*/\eta^*$. Considering also configuration #1, the ratio $B\alpha^*/\eta^*$ seems to be importantly affected by the frequency ratio (Figure 6). In fact, in the case of $\gamma_n < 1$, the centre of rotation lies in a small region downstream the midchord, as suggested by the increase of the phase angle to about 164°, and the heaving component is enhanced.

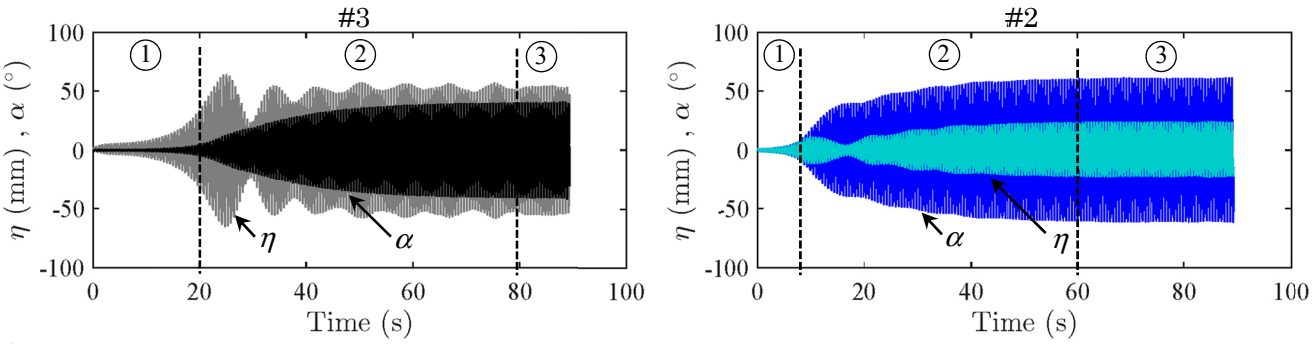

Figure 5: Build-up of flutter oscillations for symmetric (left) and mass-unbalanced (right) configurations having low heaving damping. Three phases are highlighted: 1) exponentially growing motion according to linear theory; 2) transition regime due to the activation of nonlinearities of self-excited loads and phase adjustment; 3) steady-state LCO amplitudes.

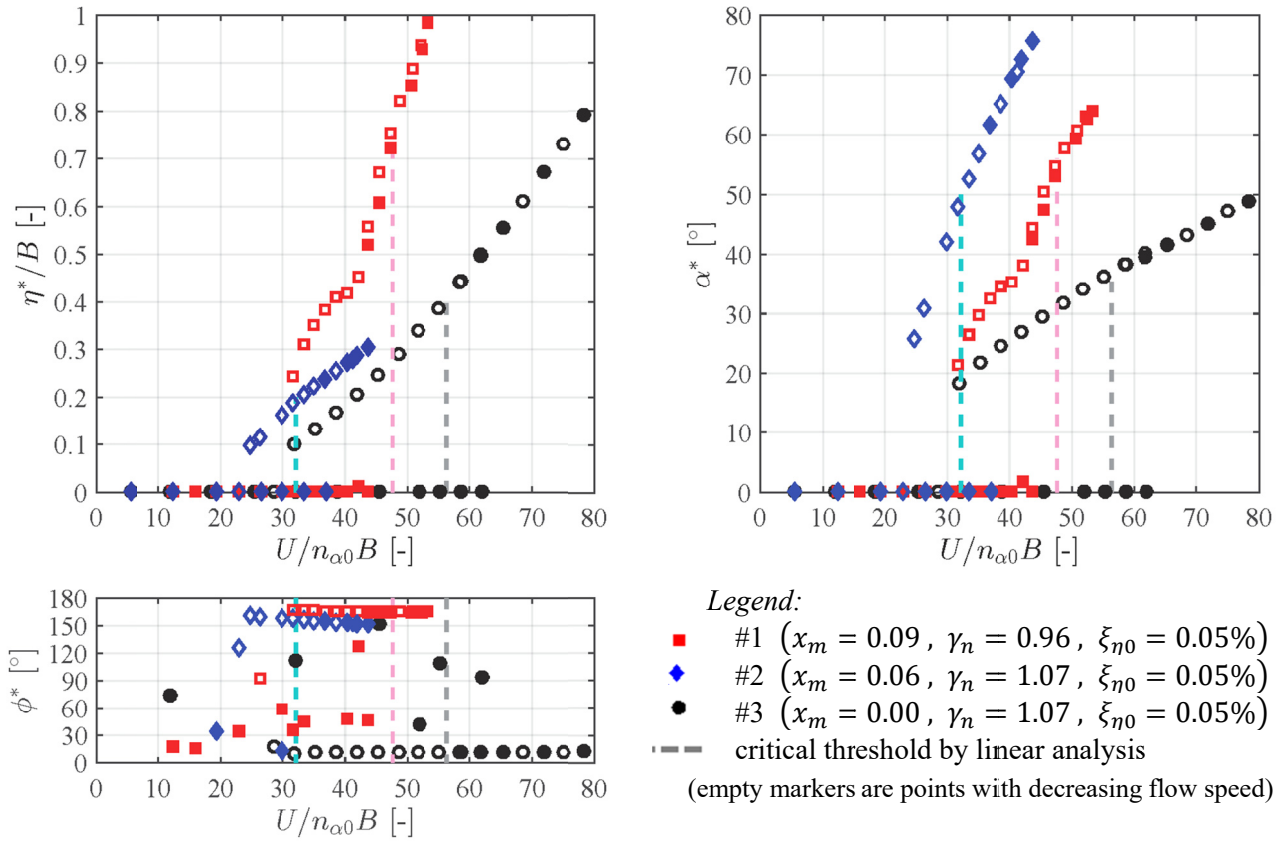

Figure 6: Comparison of amplitude-velocity diagrams for heaving and pitching components and their phase difference for the configurations with low heaving damping.

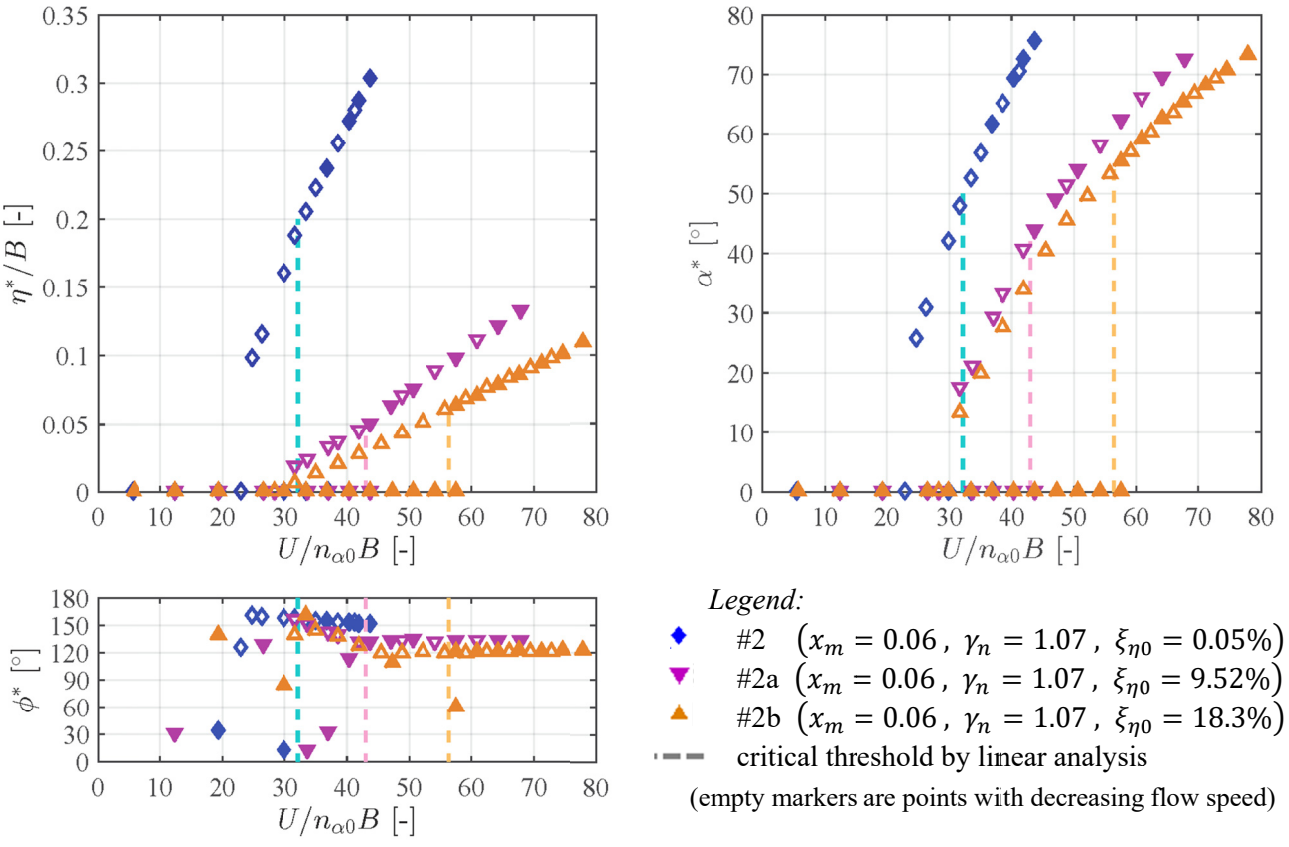

Figure 7: Effects of high levels of heaving damping on the mass unbalanced configuration.

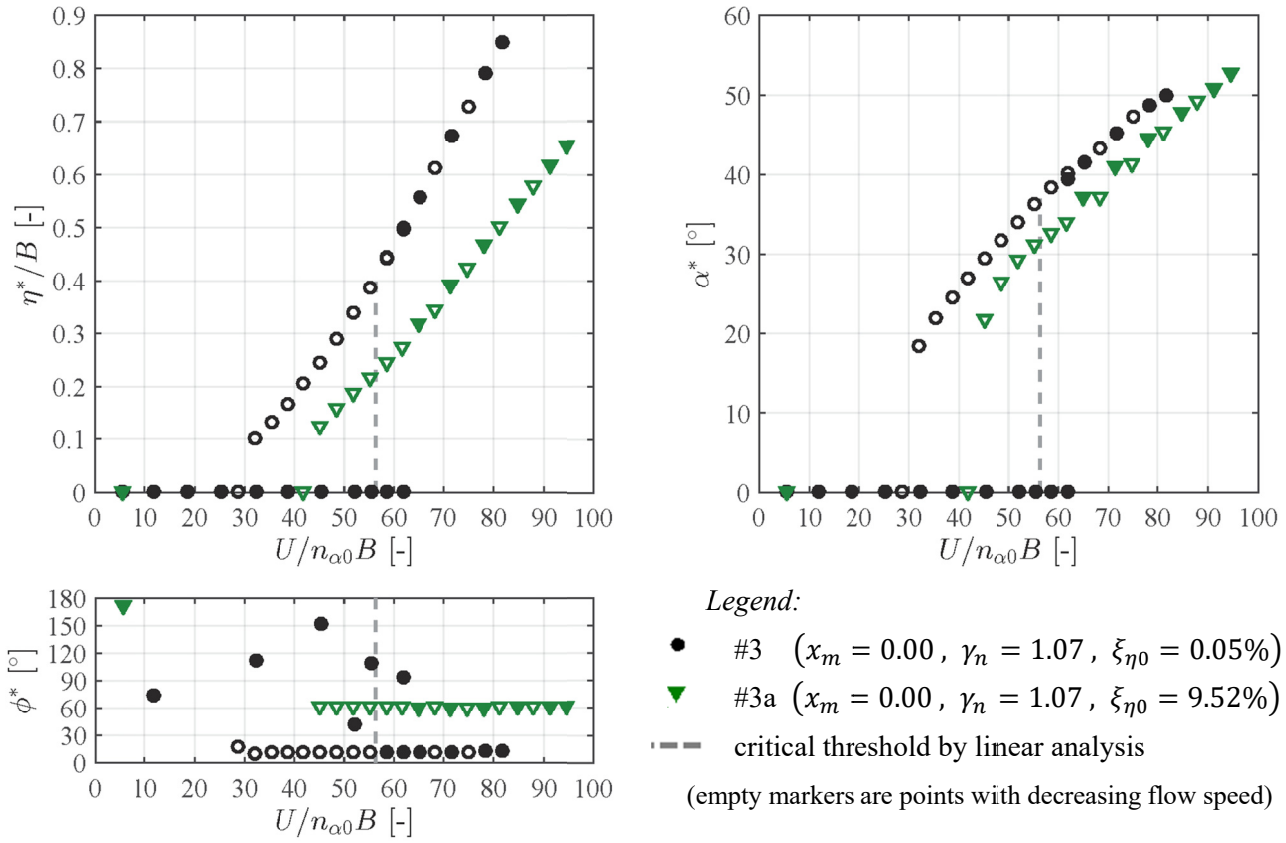

Figure 8: Effects of high level of heaving damping on the symmetric configuration. It is worth remarking that configuration #3a is stable according to the linear theory but it exhibits steady-state oscillations, if triggered by the release of large initial conditions.

In general, the increase of heaving damping nonlinearly modifies the amplitude-velocity diagrams, as shown in Figure 7. In particular, for the specific case of configuration #2, it is clear that the pitching and even more the heaving amplitudes first significantly reduce for an increment of the heaving damping from 0.05% to 9.5%. By contrast, a further increase of the damping, up to 18.3%, does not produce any dramatic reduction of the oscillation amplitude. In addition, the critical condition is postponed but the amplitude-velocity paths preserve the main qualitative features, such as the sudden jump at the instability threshold and the drop-down at the lower bound of the subcritical branch, or the nearly linear evolution with the flow speed of the sub-critical and post-critical branches.

According to the linear theory, the increase of external damping in the case of the symmetric configuration #3 fully stabilizes the system. Therefore, although configuration #3a is theoretically not prone to flutter instability, steady-state oscillations were achieved, as shown in Figure 8, provided that the system was artificially disturbed through large initial conditions, so that an amplitude-velocity diagram was obtained anyway. This result highlights the differences between the self-excited loads that dominate the steady-state regime and those responsible for the incipient classical flutter instability. In particular, while this last relies on the aeroelastic coupling between structural modes and respective fluid-dynamic reactions that leads to phase adjustment and loss of damping, when massive flow separation occurs at high angles of attack due to dynamic stall[12], the motion is governed by hysteresis loops in the nonlinear fluid-dynamic loads.

In the case of small mass unbalance (Figure 7), the phase ϕ^* decreases from about 152° for low heaving damping ($\xi_{\eta 0} = 0.05\%$) to about 133° for $\xi_{\eta 0} = 9.52\%$ and to about 121° for $\xi_{\eta 0} = 18.13\%$. By contrast, for the symmetric configuration (Figure 8) the phase angle starts from about 12° and increases up to about 61° if the heaving damping is equal to 9.52%. In general, the phase difference between pitching and heaving motions seems to tend to 90° for very high heaving damping, suggesting that the system adjusts the motion to an optimal condition while exhibiting self-sustained oscillations in the case of very high mechanical dissipation.

In all the tested configurations, the theoretical and experimental critical conditions are in good agreement. Moreover, the instability threshold always lies close to the change of slope between the sub-critical and the post-critical branch, probably suggesting a slightly different excitation mechanism in the two ranges. It is also worth noting that, even though the increase of heaving damping stabilises the system, mainly through a reduction of the motion amplitudes, the unstable branch gets closer to the rest position, so that smaller perturbations can be sufficient to foster the steady-state motion in the sub-critical range.

4. CONCLUSIONS

A systematic experimental approach was used to explore the behaviour of a flat plate model with rectangular 25:1 width-to-depth cross section prone to two-degree-of-freedom classical flutter. Analytical linear models supported the investigation of the flutter critical condition. Wind tunnel tests on a spring-mounted sectional model were conducted to verify the critical condition and to investigate the large amplitude oscillations in the post-critical regime for several dynamic configurations. The key role played by the position of the mass centre and by the damping in the translational degree of freedom was mainly studied.

A small mass unbalance significantly anticipates the instability threshold and modifies the characteristics of the motion in terms of ratio of pitching to heaving components and phase difference. For the investigated set of configurations, the introduction of high levels of heaving damping reduces the motion amplitude and postpones the instability threshold. The amplitude-velocity diagrams are not distorted by increasing the external damping, maintaining a linear evolution with the flow speed of the sub-critical and post-critical branches. By contrast, the slopes of these branches nonlinearly depend on the damping. Steady-state oscillations were found also for a configuration theoretically stable with large damping provided that the motion is artificially triggered through a large enough initial condition

The present results can form the basis for the development of numerical nonlinear models to predict large-amplitude post-critical oscillations that are triggered by the classical-flutter instability but whose evolution to the steady state is mainly driven by the dynamic-stall mechanism.

In the near future, the investigation will be extended to other dynamic parameters governing the flutter problem, in order to achieve a more complete knowledge of their influence on the post-critical flutter regime.

5. ACKNOWLEDGMENT

The authors gratefully acknowledge the contribution of Mikel Ogueta during the experimental tests.

REFERENCES

1) S. Roundy, “On the effectiveness of vibration-based energy harvesting”, *J. Intel. Mat. Syst. Str.*, vol. 16, no. 10, pp. 809-823, 2005.

2) M. M. Bernitsas, K. Raghavan, Y. Ben-Simon and E. M. H. Garcia, “VIVACE (Vortex Induced Vibration Aquatic Clean Energy): A New Concept in Generation of Clean and Renewable Energy From Fluid Flow,” *J. Offshore Mech. Arct.*, vol. 130, no. 4, pp. 041101 (1-15), 2008.

3) A. Barrero-Gil, G. Alonso and A. Sanz-Andres, “Energy harvesting from transverse galloping”, *J. Sound Vib.*, vol. 329, no. 14, pp. 2873–2883, 2010.

4) G. Ahmadi, “An oscillatory wind energy convertor”, *Wind Energy*, vol. 18, pp. 115-120, 1978.

5) L. Caracoglia, “Feasibility assessment of a leading-edge-flutter wind power generator”, *J. Wind Eng. Ind. Aerod.*, vol. 98, no. 10-11, pp. 679–686, 2010.

6) H.-J. Jung and S.-W. Lee, “The experimental validation of a new energy harvesting system based on the wake galloping phenomenon”, *Smart Mater. Struct.*, vol. 20, no. 5, pp. 055022 (1-11), 2011.

7) W. McKinney and J. De Laurier, “The Wingmill: An Oscillating-Wing Windmill”, *J. Energy*, vol. 5, no. 2, pp. 106-115, 1981.

8) K. Isogai, M. Yamasaki, M. Matsubara and T. Asaoka, “Design study of elastically supported

flapping wing power generator", in Int. Forum on Aeroelasticity and Structural Dynamics, Amsterdam, 2003.

9) Q. Zhu, M. Haase and C. H. Wu, "Modeling the capacity of a novel flow-energy harvester", *Appl. Math. Mode*l., vol. 33, no. 5, pp. 2207–2217, 2009.

10) M. Bryant and E. Garcia, "Modeling and Testing of a Novel Aeroelastic Flutter Energy Harvester", *J. Vib. Acoustics*, vol. 133, no. 1, pp. 011010 (1-11), 2011.

11) X. Amandolese, S. Michelin and M. Choquel, "Low speed flutter and limit cycle oscillations of a two-degree-of-freedom flat plate in a wind tunnel", *J. Fluid. Struct*., vol. 43, pp. 244-255, 2013.

12) Y. Fung, An Introduction to the Theory of Aeroelasticity, New York: John Wiley and Scons, Inc., 1955.

13) J. Larsen, S. Nielsen and S. Krenk, "Dynamic stall model for wind turbine airfoils", *J. Fluids Struct*., vol. 23, pp. 959-982, 2007.

14) J. Leishman and T. Beddoes, "A semi-empirical model for dynamic stall", *J. Am. Helicopter Soc*., vol. 34, no. 3, pp. 3-17, 1989.

15) D. Petot, "Modélisation du décrochage dynamique par équations différentielles", *La Recherche Aérospatiale*, vol. 5, pp. 59-72, 1989.

16) E. Dowell, R. Clark, D. Cox, H. Curtiss, J. Edwards, D. Peters, R. Scanlan, E. Simiu, F. Sisto, K. Hall and T. W. Strganac, A Modern Course in Aeroelasticity (Solid Mechanics and Its Applications), 4th ed., Klower, USA: Springer, 2004.

17) S. Bhat and R. Govardhan, "Stall flutter of NACA0012 airfoil at low Reynolds numbers", *J. Fluids Struct.,* vol. 41, p. 166–174, 2013.

18) W. McCroskey, "Unsteady airfoils", *Annu. Rev. Fluid Mech*., vol. 14, p. 285–311, 1982.

19) S. Sarkar and H. Bijl, "Nonlinear aeroelastic behavior of an oscillating airfoil during stall induced vibration", *J. Fluids Struct*., vol. 24, p. 757–777, 2008.

20) N. Razak, T. Andrianne and G. Dimitriadis, "Flutter and stall flutter of a rectangular wing in a wind tunnel", *J. AIAA*, vol. 49, no. 10, p. 2258–2271, 2011.

21) C. W. Emory, "Prediction of Limit Cycle Oscillation in an Aeroelastic System using Nonlinear Normal Modes", Blacksburg, Virginia, 2010.

22) A. Abdelkefi, R. Vasconcellos, F. D. Marques and M. R. Hajj, "Modeling and identification of freeplay nonlinearity", *J. Sound Vib*., vol. 331, no. 8, pp. 1898-1907, 2012.

23) P. Dunn and J. Dugundji, "Nonlinear stall flutter and divergence analysis of cantilevered graphite/epoxy wings", *J. AIAA*, vol. 30, no. 1, p. 153–162, 1992.

24) L. Pigolotti, C. Mannini, G. Bartoli and K. Thiele, "Wind tunnel tests on elongated rectangular plates under flutter motion: limit-cycle oscillations and preliminary energy harvesting considerations", in Proc. of 14th Int. Conf. on Wind Engineering, Porto Alegre, Brazil, June 21-26, 2015.

25) M. Karami, M. Amin and J. Daniel, "Equivalent damping and frequency change for linear and nonlinear hybrid vibrational energy harvesting systems", *J. Sound Vib*., vol. 330, no. 23, pp. 5583-5597, 2011.

26) M. Matsumoto, "Aerodynamic damping of prisms", *J. Wind. Eng. Ind. Aerod*., vol. 59, pp. 159-175, 1996.

27) R. Bisplinghoff and H. Ashley, Principles of Aeroelasticity, NewYork: John Wiley and Sons, Inc., 1962